

# A Compact Dental Robotic System Using Soft Bracing Technique

Jing Li, Zhong Shen<sup>ID</sup>, Wen Yu Tian Xu, Walter Yu Hang Lam, Richard Tai Chiu Hsung, Edmond Ho Nang Pow, Kazuhiro Kosuge, and Zheng Wang<sup>ID</sup>

**Abstract**—A wide range of commonly performed dental procedures, from operative caries removal, crown preparation, filling, to Orthodontia, could potentially benefit from robotic assistance or enhancement. Despite the wide applicability, dental robots have received far less research attention in comparison with surgical robots in general, with the vast majority of state-of-the-art dental robot systems built around commercially available industrial robotic manipulators. In this letter, we propose a novel robotic manipulator system dedicated to dental applications. The proposed robot design utilizes tendon-sheath transmission, by which the electric-motor actuators could be placed away from the manipulator, resulting in substantially more compact size and lighter weight than industrial-arm-based state-of-the-art systems. The main contribution of this letter is introducing a soft-robotic bracing element, which could substantially improve manipulator performance including stiffness, force capability, and accuracy. The concept, design, and fabrication aspects of the soft bracer are presented in detail in this letter. Design and system integration of the entire dental robot system are also introduced, and the performance of the system is validated using a fabricated prototype, where the benefits and unique performances of using the soft bracer are highlighted from experimental results. With compact size, excellent tool interchangeability, and fully customized toward dental procedure specifications, the proposed dental robot system with soft bracer could potentially be used in wide applications from caries removal to crown treatments, offering a promising alternative with substantially smaller footprint and lower cost to current solutions.

**Index Terms**—Tendon/wire mechanism, medical robots and systems.

Manuscript received September 10, 2018; accepted January 4, 2019. Date of publication January 23, 2019; date of current version February 15, 2019. This letter was recommended for publication by Associate Editor M. Zecca and Editor P. Valdastri upon evaluation of the reviewers' comments. This work was supported in part by Hong Kong RGC-ECS Grant 27210315, in part by Shenzhen Basic Research Programme JCYJ20150629151046885, in part by ITF Grants ITS/140/18 and ITS/457/17FP, and in part by HKU Seed Funds 201611159196 and 201611160034. (*Corresponding author: Zheng Wang.*)

J. Li, Z. Shen, and W. Y. T. Xu are with the Department of Mechanical Engineering, The University of Hong Kong, Hong Kong (e-mail: lijingtsinghua11@gmail.com; shenzhong1911@gmail.com; xuwenyutian@gmail.com).

W. Y. H. Lam and E. H. N. Pow are with the Faculty of Dentistry, The University of Hong Kong, Hong Kong (e-mail: retlaw@hku.hk; ehnpow@hku.hk).

R. T. C. Hsung is with the School of Information Engineering, Guangdong University of Technology, Guangzhou 510006, China (e-mail: tchhsung@gdut.edu.cn).

K. Kosuge is with Department of Robotics, Tohoku University, Sendai 980-8577, Japan (e-mail: kosuge@irs.mech.tohoku.ac.jp).

Z. Wang is with the Department of Mechanical Engineering, The University of Hong Kong, Hong Kong, and also with the Department of Mechanical and Energy Engineering, Southern University of Science and Technology, Shenzhen 518055, China (e-mail: zwangski@hku.hk; wangz@sustc.edu.cn).

Digital Object Identifier 10.1109/LRA.2019.2894864

## I. INTRODUCTION

DENTAL issues are quite common in our daily life. According to the data provided by WHO [1]–[3], 60~90% of school children and almost 100% of adults were suffering from dental caries worldwide. While severe periodontal disease has been found in 15~20% of adults at the age from 35 to 44. For elderly people from 65 to 74 years old, 30% have lost all their natural teeth. Dental issues can be extremely severe and painful, and further affect life quality and systemic health [4] if patients cannot get appropriate treatments in time. However, global labor shortage in dentistry has made timely treatments impossible for most patients. It has been reported that there are only around 2000 registered dentists in Hong Kong with 7 million populations [5], and this unbalance between demands and needs is even worse in underdeveloped regions. Long period of training makes it difficult to have enough dentists in a short time. We therefore came up with the idea of applying robots in dental procedures. With the controllable motions, robots can not only improve the efficiency of dental procedures, but also improve the treatment efficacy by preventing human errors since most dental procedures are fully dependent on dentists manual skills for now [6].

Robots in dentistry can be generally divided into two categories [7], [8], one is for training purposes by simulating human reactions during dental treatments [9]–[12], and the other is for assisting dental procedures [13]–[16]. For the latter one, multiple designs have been proposed for different dental procedures [17], [18], among which, Yomi, released by Neocis Company and the dental robot developed [19] are the most advanced ones. Yomi was approved by FDA in 2017 and is targeted at dental implants surgeries. With its navigating system, Yomi is able to provide a physical guidance for dentists to precise localization of the tooth needing repair. While the dental robot proposed [19] has performed a clinical trial of dental implant surgery, where the robotic manipulator is able to locate to the dental caries automatically.

Both of these manipulators were adapted from current industrial manipulators, whose dimensions as well as workspaces are far more than enough for dental applications [20]. In our design, we applied tendon-sheath mechanism, by which the actuation part can be moved away from the joints, therefore the scale and weight of the proposed manipulator can be greatly decreased, and so is the workspace. However, unavoidable elongation of tendons, brings vibrations at the end, which will affect the performances especially when precision and steadiness are both required.

Bracing strategy for manipulator operations have been proposed and validated since 1980s [21]–[23]. Studies have shown that by sacrificing one or more degrees of freedom, the payload, stiffness and relative parts positioning accuracy can be

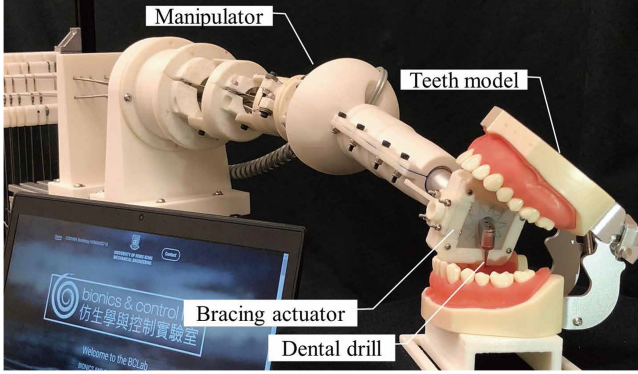


Fig. 1. Proposed dental manipulator integrated with the bracing actuator.

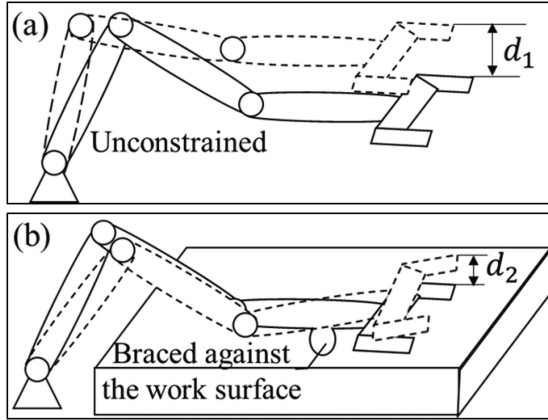


Fig. 2. Bracing strategy for manipulator operations (a) Unconstrained. (b) Braced against the work surface.  $d_i$  represents the amplitude of vibration in different conditions.

significantly improved, especially for applications such as grinding and assembly. Inspired by existing bracing strategies, we also added bracing structure in the proposed system in order to obtain better performances. Different from previous designs as rigid bracing structure, we applied a soft bracing actuator made of silicone gel, the shape of which will change depending on the input air pressure. With the soft bracing actuator, the stiffness of the proposed system has increased and more flexibilities remained compared with those with rigid bracing structures.

Bracing strategy will be explained in details in section II. In section III, the whole system design and kinematics analysis will be elaborated. Control and integration of the robotic system will be introduced in section IV. Experiments validation will be illustrated in section V, including experimental instruments and results. In the last section, summary of our work and possible future applications can be found.

## II. BRACING STRATEGY

Bracing to increase positioning accuracy and stiffness can be easily understood as similar to humans handwriting motions with elbows or wrists contacting the table surface. In terms of robot operations, bracing strategies have also been used to improve robot performances. Basic idea of bracing is to add restrictions to some point of the manipulator other than the end-effector, among which, bracing against a surface has been widely used as shown in Fig. 2(b) [21].

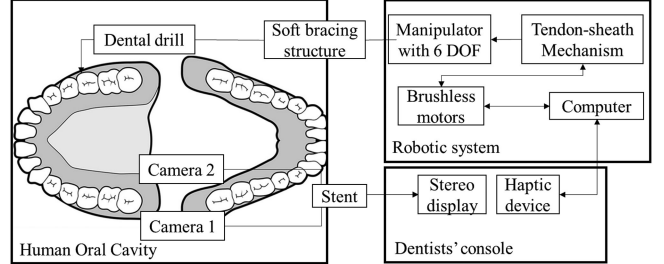


Fig. 3. Scheme of proposed robotic system.

Undesirable vibrations usually occur during robot operations due to the compliance between joint connections, especially for manipulators with multiple degrees of freedom. For tasks requiring precision, it takes extra time waiting for the vibration to be damped out which limits the force and position control [21] at the end-effector. It became worse for machining and drilling procedures, where the vibratory load could excite a resonance if the lowest natural frequency is not sufficiently higher than the load vibrating frequency.

Dynamic behaviors of the braced and non-braced manipulator have been analyzed [21], which has validated that the lowest natural frequency of the braced manipulator is always larger than or at least equal to non-braced ones, the dynamic performances of manipulators can therefore be improved with bracing structures.

## III. SYSTEM DESIGN AND ANALYSIS

### A. System Design

The robotic system we proposed consists of three parts, a braced manipulator of 6 degrees of freedom, with a commercially available dental drill as the end-effector, 6 motors for motion control, and a dentist console, including an imaging system and a haptic device for teleoperation. The system scheme is presented in Fig. 3. All the joints were 3D printed by plastic filaments (PLA+). Motors (DYNAMIXEL) are connected to joints by tendon-sheath mechanism and one motor for one joint. During procedures, dentists hold the haptic device (Touch 3D Stylus) which provides its end position in real time, the manipulator will move in the same trajectory as the haptic device by sending appropriate instructions to motors. And the scheme of the proposed system can be found in Fig. 3.

### B. Kinematics Analysis

The proposed robotic manipulator consists of six joints, including two revolute joints, two cylindrical joints and one wrist joint with two joints crossed. Detailed mechanical design specifications can be found in Table II. The resolution of joint angle as well as the joint continuous output torque is calculated according to the technical specifications of motors (DYNAMIXEL MX series and PRO series). The motion and force transmission results are considered and converted as well. The position accuracy was calculated in three dimensions as x, y, z, according to their relations between joint angles. The steel wires elongation was estimated by calculating the elastic elongation of steel wires with total length as 350mm, diameter as 0.68mm and under 300g load. Both of these results are shown in Table II. DH parameters are listed in Table I.

TABLE I  
DH PARAMETERS

Link i	$\alpha_{i-1}$	$a_{i-1}$	$d_i$	$\theta_{i-1}$
1	0	0	$l_0$	$\theta_1$
2	-90°	0	0	$\theta_2$
3	0	$l_3$	0	$\theta_3$
4	90°	0	$l_4$	$\theta_4$
5	-90°	0	0	$\theta_5$
6	-90°	0	0	$\theta_6$
Tool	90°	$-l_7$	$l_6$	-90°

TABLE II  
SYSTEM PARAMETERS

Dimension (mm)	Rotational range(°)		Joint angle resolution(rad)		Joint continuous output torque(Nm)	
$l$	436.32	$\theta_1$	0 ~ 360°	$\Delta\theta_1$	0.0004	$J_1$
$l_0$	85.79	$\theta_2$	0 ~ 105°	$\Delta\theta_2$	0.0004	$J_2$
$l_3$	53.66	$\theta_3$	0 ~ 132°	$\Delta\theta_3$	0.0005	$J_3$
$l_4$	81.72	$\theta_4$	0 ~ 360°	$\Delta\theta_4$	0.0023	$J_4$
$l_6$	200.20	$\theta_5$	0 ~ 90°	$\Delta\theta_5$	0.0002	$J_5$
$l_7$	26.88	$\theta_6$	0 ~ 90°	$\Delta\theta_6$	0.0002	$J_6$
$d$	155.45	Accuracy(mm)		Wire elongation(mm)		
$d_0$	100.00	$\Delta x$	0.045	$\Delta y$	0.045	$\Delta z$
					0.047	0.018

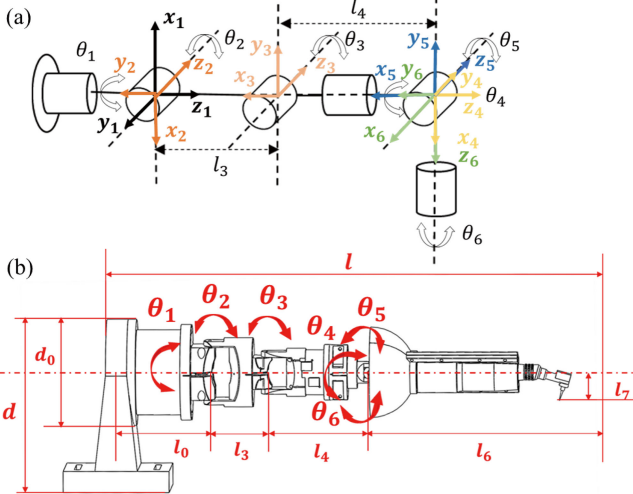


Fig. 4. Design of the proposed manipulator. (a) Coordinate frames of the proposed manipulator. (b) Joints of the proposed manipulator.

Transformation matrixes can be written according to DH parameters and the position of the last joint can be computed by multiplying these transformation matrixes in order. We assume the starting point is  $(0, 0, 0, 1)^T$  labeled as  $(x_0, y_0, z_0)$  in Fig. 4 and the center position of the last joint is shown below.

$$x_6 = c\theta_1(l_3c\theta_2 + l_4s\theta_2) \quad (1)$$

$$y_6 = s\theta_1(l_3c\theta_2 + l_4s\theta_2) \quad (2)$$

$$z_6 = l_4c\theta_2 + l_3s\theta_2 + l_0 \quad (3)$$

Regarding inverse kinematics analysis, the position and orientation of the 6<sup>th</sup> joint is assumed to be  $(x_6, y_6, z_6, \alpha_6, \beta_6, \gamma_6)$ , through which the angles of each joint can be calculated. Since the last three joints intersect with each other, the location of the last joint only relates to the first three joints. And the results are

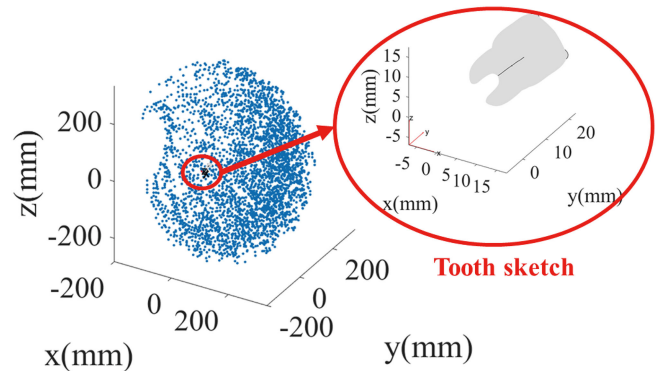


Fig. 5. Workspace of the proposed manipulator in 3 dimension with a modular tooth sketch.

as follows.

$$\theta_1 = 2 \arctan \frac{-x_6 \pm \sqrt{x_6^2 + y_6^2}}{y_6} \quad (4)$$

$$\theta_3 = 2 \arctan \frac{2l_3l_4 \pm \sqrt{4l_3^2l_4^2x_6^2 - (r^2 - l_3^2 - l_4^2)}}{x_6^2 + y_6^2 + z_6'^2 - l_3^2 - l_4^2} \quad (5)$$

$$\theta_2 = 2 \arctan \frac{-(l_4s\theta_3 + l_3) \pm \sqrt{l_3^2 + l_4^2 - z_6'^2 + 2l_3l_4s\theta_3}}{z_6' + l_4c\theta_3} \quad (6)$$

Where  $z_6' = z_6 - l_0$ ,  $s\theta = \sin\theta$ ,  $c\theta = \cos\theta$ ,  $r^2 = x_6^2 + y_6^2 + z_6'^2$ .

The rest of the joint angles can be calculated based on the rotational transformation matrix  ${}^3_6 R$ , which can be computed according to  ${}^3_6 R = {}^3_3 R {}^T {}^0_6 R$ .

Based on the kinematics analysis, the workspace of the proposed manipulator is plotted as shown in Fig. 5, where the angle ranges of the cylindrical joints are 90 degrees, for the rest joints are half of its full rotational range. A human tooth sketch is plotted in Fig. 5, which can be fully covered by the workspace of the dental drill mounted on the proposed manipulator.

### C. Tendon-Sheath Mechanism

Tendon-sheath mechanism has been widely used in surgical robots [24]–[27], especially in laparoscopic surgeries, where space constrains can be greatly relieved by moving actuation parts away. Similar in our case, tendon-sheath mechanism has brought us more flexibilities in manipulations in dental procedures.

Structures of joints were designed based on its motion features, therefore we have three types of joints, which are cylindrical joint, revolute joint and wrist joint. Similar to our previous work published in [28], both of the cylindrical joints consist of two parts, the outer part and the inner part which rotates along the center shaft and transfers the rotatory motion to its proximal joints. A pair of tendons are used to connect these two parts and actuate rotations in clockwise and counterclockwise directions as shown in Fig. 6(a) and (c). Revolute joint as shown in Fig. 6(b) rotates around the shaft perpendicular to both of its distal and proximal end. A pair of tendons is placed mirror symmetrically

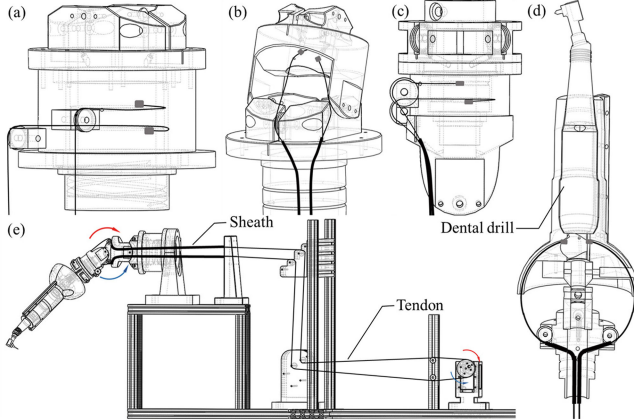


Fig. 6. Tendon-sheath mechanism of the proposed manipulator. (a) First cylindrical joint. (b) First revolute joint. (c) Second cylindrical joint. (d) Wrist joint. (e) Tendon-sheath mechanism of the whole system. Bold black lines represent the tendons covered with sheath, while black lines represent tendons.

passing through the holes in the distal and proximal end. And the other revolute joint differs only in size.

The wrist joint was designed based on a universal joint. The two ends of the universal joint were fixed to two separate parts, and were connected with four wires, one for each direction. In order to prevent the interferences between wires crossed in between, the moving trajectories of wires are restricted to a sphere whose center is the same as the universal joint. When one wire is stretched, the other wire opposing to it will be loosened, and the crossed ones will not be affected since the motion generated is along the surface perpendicular to them.

#### D. Soft Bracing Actuator Design

In order to increase the stiffness of the proposed system, we applied bracing strategy as well. Conventional bracing strategy with rigid structures increases control complexity as well as constrains in workspace. Inspired by soft robots with controllable compliance [29], [30], we braced the proposed manipulator with a soft actuator as shown in Fig. 7(f). Different from the soft bending actuators described before [31]–[33], the proposed soft bracing actuator is specialized for giving the dental drill a human-friendly supporting point inside the mouth. Therefore, three major requirements have to be satisfied: a) a ring-shaped actuator outline is needed to cover the dental drill so that force applied on the drill is isotropic; b) when the soft bracing is inflated, the part that covers the dental drill should expand towards the center while the other parts remain the same; c) the soft bracing actuator should be large and stiff enough to keep the mouth open, but not too large to block the camera or to damage a persons mouth. Also, two silicone rubber (Dragon skin 10 & 30, Smooth-on Inc., PA, USA) with different elasticity modulus were chosen for comparison. Inner layer was first molded using a ring-shaped 3D printed part to define the chamber (Fig. 7(a)). Strain limiting mesh was winged on both top and bottom of inner layer using fiber reinforcement (Fig. 7(b)). The part was then put into a second set of 3D printed mold for outer layer molding. (Fig. 7(c)). The outer layer shape was based on a standard trapezoid mouth opener. When the silicone was cured, the ring-shaped part was removed and a set of 3D printed clamp was added onto the actuator (Fig. 7(d)), which served the purpose

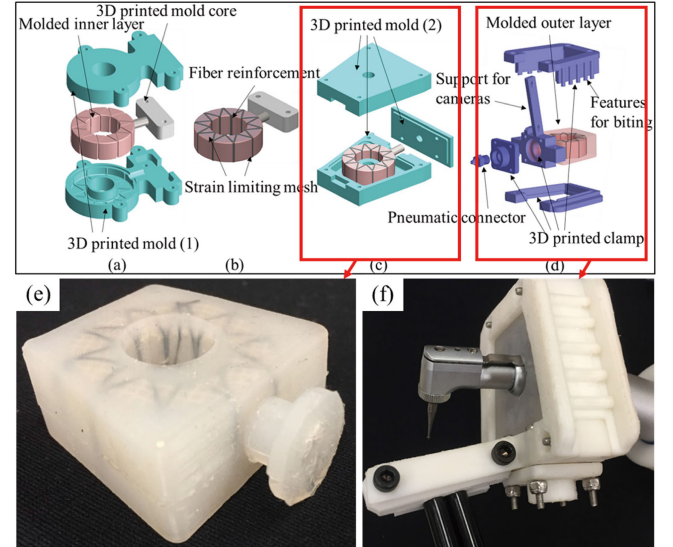


Fig. 7. Design and fabrication of the soft bracing actuator. (a) Inner layer molding using 3D printed mold (1). (b) Adding strain limited mesh by winding fiber reinforcement. (c) Outer layer molding using 3D printed mold (2). (d) Removing ring-shaped part and adding clamp. (e) Soft bracing actuator. (f) Soft bracing actuator with cameras and the dental drill.

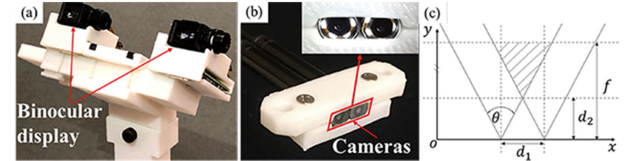


Fig. 8. Stereo imaging system. (a) Binocular display. (b) Cameras. (c) Scheme of the imaging system,  $d_1$  is the distance between two lenses, which is limited to the geometry of the cameras as 5.5mm,  $f$  is the focal length of the lens in cameras as 20mm,  $\theta$  is the angle of view of the camera as 56° and  $d_2$  is the minimum distance between the object and the cameras in order to have stereo imaging as around 5.2mm. Hatched area shows the overlapping area of the two view-fields, where a clear stereo imaging can realize.

of both sealing and constrain of side wall expansion, as well as supporting cameras.

#### E. Imaging System

The imaging system contains two cameras positioned close to teeth and a binocular display for dentists to monitor the locating and drilling process during procedures. The configuration of these two cameras are shown in Fig. 8. The distance between the two displays can be adjusted in order to fit pupil distance of different people.

## IV. CONTROL AND SYSTEM INTEGRATION

In this section, the control method of the whole system will be presented (Fig. 9), especially the teleoperation part. The configuration of the whole system will be shown as well.

The haptic device in the proposed system consists of 6 degrees of freedom, and the position and orientation of its end-effector can be obtained through its built-in sensors, which has been used for position mapping in teleoperations for the proposed system. The configuration of the haptic device is shown in Fig. 10(c), while the configuration of the proposed manipulator can be found in Fig. 10(a). Based on the position mapping in Cartesian

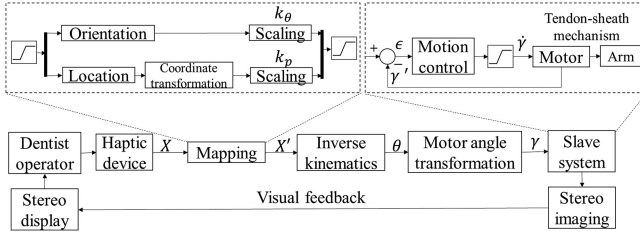


Fig. 9. Control scheme of the proposed system.  $X$  represents the position and orientation of the haptic device,  $X'$  is the corresponding result including position and orientation after mapping which can be used for inverse kinematics analysis for joint angle  $\theta$ .  $\gamma$  represents the motor angles computed based on the motion transmission experimental results, while  $\dot{\gamma}'$  is the real motor angle obtained through built-in encoders of motors.  $\dot{\gamma}$  represents motor velocity.

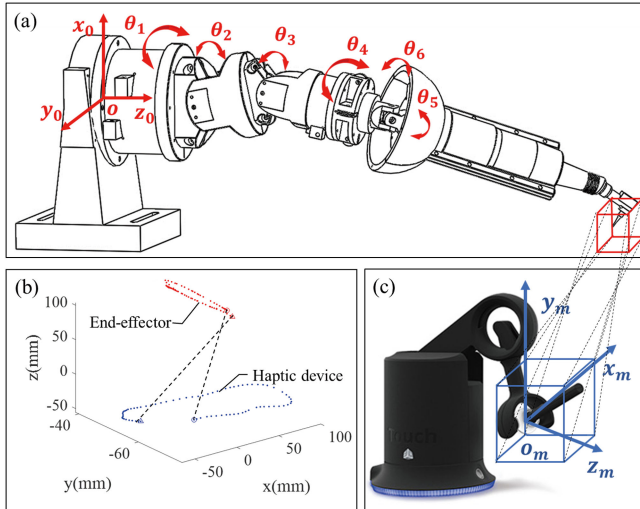


Fig. 10. Mapping between the haptic device and the proposed manipulator. (a) Scheme of the manipulator, where  $o$  represents its origin. (b) Trajectory of the end-effector of both the haptic device and the proposed manipulator end-effector after mapping. (c) Scheme of the haptic device, where  $o_m$  represents its origin.

coordinate system, the slave system including the motors, the robotic arm, can replicate the motions of the master system containing the haptic device which is operated by the dentist. The dentist can adjust his motions based on the visual feedback from the stereo imaging system.

Instead of exhausting the whole workspace of the haptic device, only a cubic-shaped volume marked as blue box in Fig. 10(c) is chosen to map to a similar cubic-shaped volume marked as a red box in Fig. 10(a) of the manipulator workspace. Only when the wrist point of the haptic device is moved into the chosen cubic volume, the position and orientation of its end will be tested valid and converted to nonzero velocity instructions to motors, otherwise, the whole system will stay in place. Coordinate system is rotated and the origin is translated in order to match the configuration of the proposed manipulator. The motions are scaled down by multiplying a factor less than one marked as  $k_p$  to the displacement between neighboring positions of the haptic device, while the orientations are multiplied by another factor as  $k_\theta$ . Confined motions as well as preserved orientations can be realized by adjusting these two scaling factors. The converted locations and orientations after mapping will be boundary test will be performed for limiting the final position

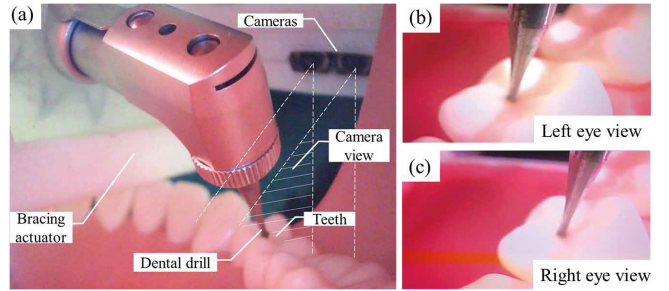


Fig. 11. Human teeth model with the proposed bracing actuator and cameras from intraoral view.

of the end-effector of the proposed robotic arm within a small range. Fig. 10(b) presents the trajectories of the end-effector and the haptic device after mapping.

Joint angles are then converted to motor angles based on the resolution of each motor and the relation between the motor angle and joint angle measured in motion transmission experiments. The motors are set to the velocity control mode, the velocities of which are determined by the differences between target motor angles and real motor angles  $\dot{\gamma}'$  and are processed with appropriate motion control. More advanced control method can be applied for better performances.

The manipulator we proposed integrated with the soft bracing actuator as well as the imaging system is shown in Fig. 11. Diameters of the two cameras we used are 5.5mm, and the focal lengths are 20mm which are fit for human oral cavity. The light intensity of LEDs integrated with the cameras can be adjusted, which makes it more convenient in dental procedures. As shown in Fig. 11, the cameras are fixed to a stent with the bracing actuator while the manipulator can move freely.

## V. EXPERIMENTAL VALIDATION

In this section, experimental setup and results will be illustrated, including motion and force transmissions, stiffness tests with and without bracing actuator, with same bracing actuator but under different air pressures and different directions and with bracing actuators made of different materials.

### A. Motion and Force Transmission

The relations between motor angles and joint angles were measured as described before [28]. The experimental results of the first four joints are shown in Fig. 12. From Fig. 12 we can see that the relation between the motor angles and joint angles can be fitted well with linear relations and the coefficients differ due to the different diameters of the mounting parts for motors and different dimensions of joints.

For cylindrical joints, the diameter of the mounting parts are 36mm, while for revolute joints and wrist joints, the diameters are 12mm. In order to increase the positioning accuracy and output payload as well as considering the space limitations, the diameters of the revolute joints along the rotational directions are 50mm, 60mm respectively, 47mm and 27mm for two cylindrical joints, and 80mm for the wrist joint. The ratio differences can be seen from the motion transmission measurement results as well.

The relations between input torque and output torque were measured in the same way as described in [28]. The results of the first four joints are shown in Fig. 13, where the speed ratio

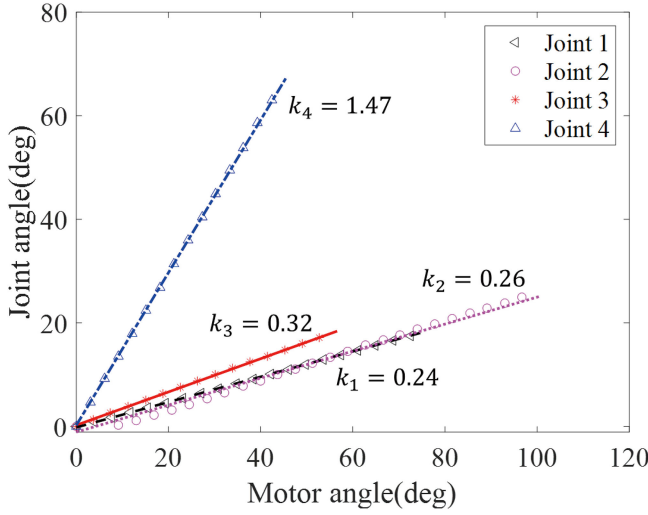


Fig. 12. Motion transmission measurement results,  $k_i$  represents the  $i^{th}$  joint coefficient.

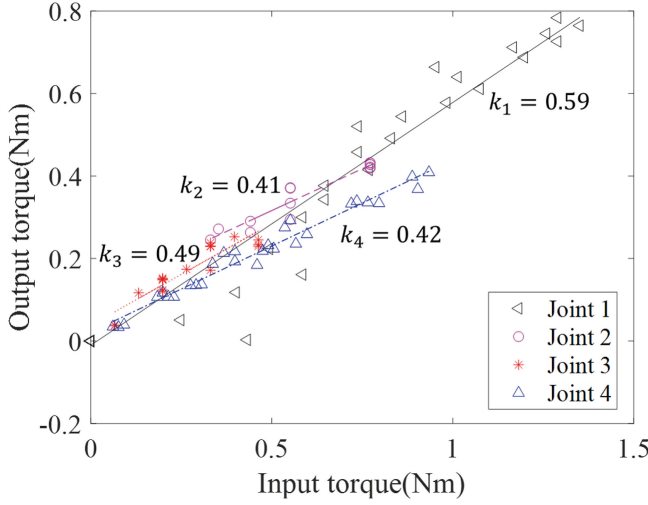


Fig. 13. Force transmission measurement results,  $k_i$  represents the  $i^{th}$  joint coefficient.

between motors and joints have been considered and converted. Therefore the data reflects the energy loss owing to the friction between tendon and sheath. From the data obtained, around 50% of the input torque have been lost during the transmission.

#### B. Stiffness Tests Under Different Conditions

In order to verify performances of the braced manipulator, stiffness at the end-effector has been measured. The experimental setup can be found in Fig. 14, where the force sensor and the linear encoder were installed on either side of dental drill. When the dental drill is pushed by the force sensor, the linear encoder will record the displacement under such force, therefore the relation between the force and displacement can provide us the stiffness of this configuration.

Stiffness tests with and without the bracing actuator were performed and the results are shown in Fig. 15, which displays a great improvement to stiffness after adding the bracing actuator to the system. The middle three lines show the stiffness under different air pressures with the same bracing actuator made of

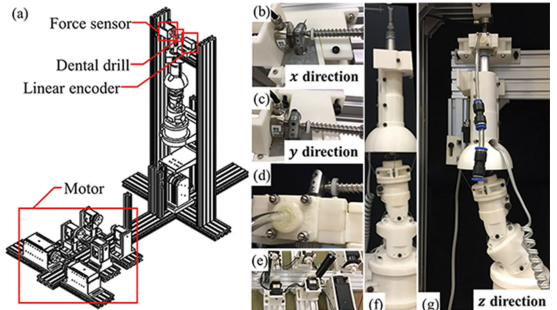


Fig. 14. Experimental setup for stiffness tests. (a) Overall setup. (b) Setup of stiffness test in  $x$  direction. (c) Setup of stiffness test in  $y$  direction. (d) Setup of motion transmission test. (e) Motors. (f) Manipulator in upright position. (g) Manipulator in zigzag position, for stiffness test in  $z$  direction.

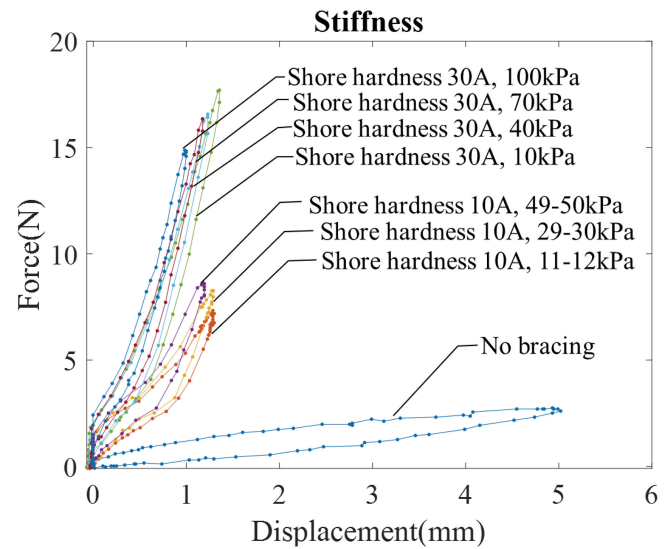


Fig. 15. Stiffness measurement results under different configurations.

Dragon skin 10 with shore hardness as 10A, while lines at the left side present the stiffness with the bracing actuator made of Dragon skin 30 with shore hardness as 30A, a stiffer material. It is obvious that higher the air pressure is, larger the stiffness will be. And for stiffer material, larger air pressure differences are needed to cause similar stiffness differences, which is corresponding to the common sense that stiffer materials are harder to deform. And stiffness results for the softer materials are smaller than the stiffer one.

From the results shown in Fig. 15, we can conclude that it is effective to apply bracing to increasing system stiffness. In our case, changing materials and air pressure can both affect the stiffness and stiffer materials are more effective than enlarging air pressure.

Stiffness of braced manipulator in different directions have been measured as well with two bracing actuators made of different materials. The setup configurations can be found in Fig. 16. Three directions perpendicular to each other were chosen and labeled as  $x$ ,  $y$  and  $z$  in Fig. 14. As shown in Fig. 16, we can find that the stiffness in  $z$  direction is much larger than those in the other two directions, which also corresponds to the configuration of the proposed manipulator, whose size in  $z$  direction is much larger than in  $x$  and  $y$  directions. The stiffness in  $x$  and  $y$  directions is similar to each other for both bracing

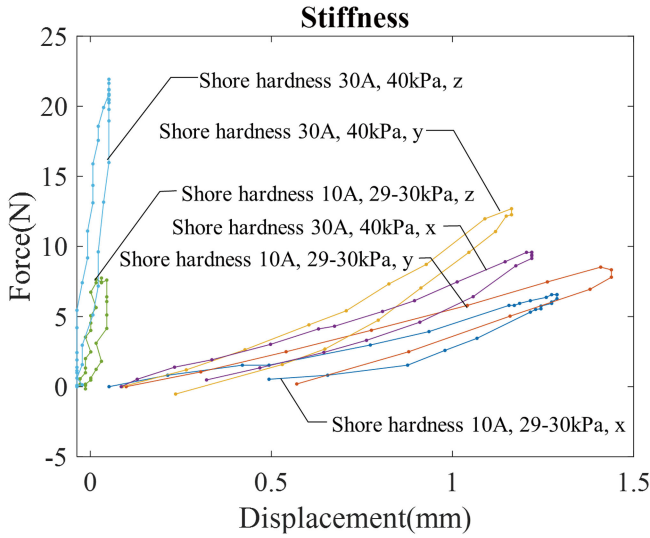


Fig. 16. Stiffness measurement results with bracing actuator in different directions.

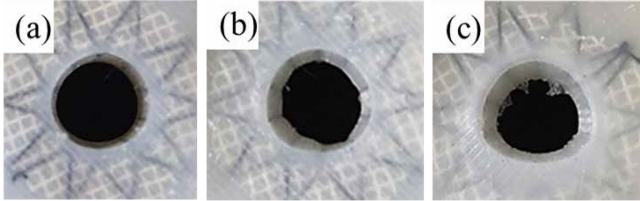


Fig. 17. Soft bracing actuator. (a) No air inflation. (b) Soft bracing actuator made of Dragon skin 30 with air inflation. (c) Soft bracing actuator made of Dragon skin 10 with air inflation.

actuators but slightly larger for the stiffer one. In addition to the different deformation features for different materials, the asymmetry generated when applying air pressure as shown in Fig. 17 might be another reason.

### C. Motion Transmission With Bracing Actuator

Owing to the soft bracing actuator, the manipulator can still move under air inflation but the motion transmission will certainly be affected. In order to quantify these effects, motions actuated by motors and displacements under air inflation along a certain direction with soft bracers made of two materials and under different air pressures were measured. The results are shown in Fig. 18 and Fig. 20. In agreement with the stiffness results, the motion has been affected by the bracing actuator and the one made of stiffer materials affects more. Motions actuated by motors have decreased and based on these results, we simulated the workspace under the softer bracing actuator and compared it with the one without bracing as shown in Fig. 19. As labeled, the red dots represent the positions the manipulator with last three joints restricted can reach, while yellow dots are the positions the manipulator with the proposed soft bracing actuator can reach, and the blue dots show the workspace of the non-braced manipulator, through which, we can have an idea of how much the soft bracing actuator will influence on the workspace and how much it could save compared with a rigid one.

The effect of the soft bracing actuator on the position accuracy has been tested with the same experimental configuration

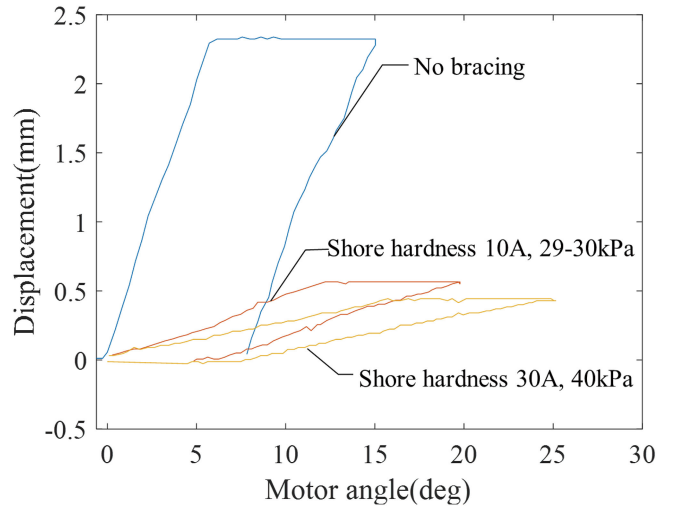


Fig. 18. Displacement measurement results with and without bracing actuator actuated by motors.

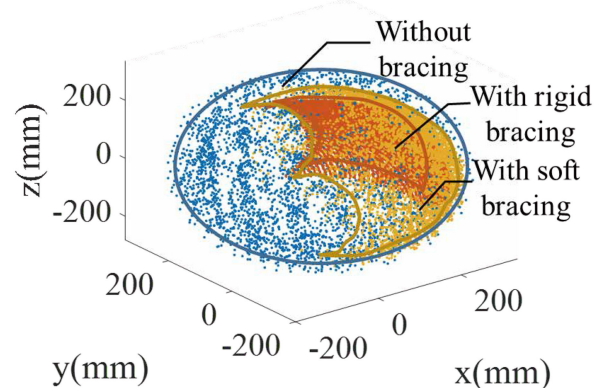


Fig. 19. Workspace simulation results with rigid and soft bracing structure and without bracing structure based on previous displacements results.

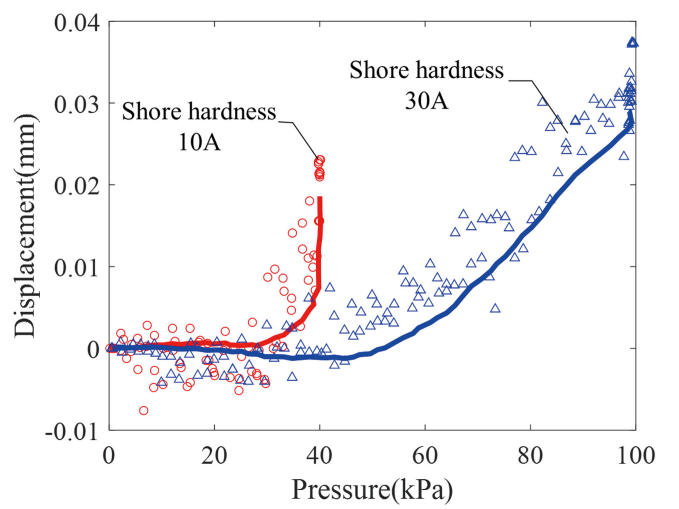


Fig. 20. Displacement measurement results with the bracing actuator under different air pressures.

as shown in Fig. 14(d), by measuring the displacement under different air pressures along one direction. Three tests were performed for both of the soft bracers. In considerations of the bracers tolerance, the air pressure added to the softer bracer is limited to 40kPa, while the air pressure added to the stiffer bracer is limited to 100kPa. During the experiments, the air pressure is increased stepwise as 100 Pa per 0.1 second by an air pump, while the linear encoder with the resolution of 0.015mm records the displacements continuously. Raw data of displacements were firstly averaged for each pressure level as plotted in Fig. 20, where the blue dots are from the dataset of the stiffer bracer, and red dots are from the softer bracer, and the lines are the fitting results corresponding with the dots of the same color.

Based on the experimental results, the effect of the soft bracing actuator on position accuracy can be ignored since the maximum displacements happening under the maximum allowable air pressure for both the stiffer and softer bracers, are within 0.04 mm, which doesn't exceed the system resolution as 0.047 mm.

## VI. CONCLUSION

In this letter, we proposed a robotic system for assisting dental drilling procedures. Different from existing dental robots, our design is specialized for dental applications, the dimension and workspace of which are much smaller, around twice smaller but sufficient for dental procedures. The soft bracing actuator we applied has significantly improved the system stiffness, which could be at least 10 times higher than the non-braced system, and different materials and air pressure have different effects on the stiffness. In general, the stiffer the material is and the higher the air pressure is, the larger the stiffness will be. The dentists console is composed of a haptic device for motion control and a stereo imaging system for monitoring the whole process.

Our dental robotic system is intended for relieving burdens of dentists, improving the efficiency of dental procedures, and reducing human errors during treatments. With several iterations of the design and algorithm, clinical trials could be conducted in the future. Hopefully, the robotic system we proposed could accelerate automation in dental treatments and further solving the problems in dentistry.

## REFERENCES

- [1] T. Vos *et al.*, “Global, regional, and national incidence, prevalence, and years lived with disability for 301 acute and chronic diseases and injuries in 188 countries, 1990–2013: A systematic analysis for the global burden of disease study 2013,” *The Lancet*, vol. 386, no. 9995, pp. 743–800, Aug. 2015. [Online]. Available: [https://doi.org/10.1016/S0140-6736\(15\)60692-4](https://doi.org/10.1016/S0140-6736(15)60692-4)
- [2] N. Kassebaum *et al.*, “Global burden of severe periodontitis in 1990–2010: A systematic review and meta-regression,” *J. Dental Res.*, vol. 93, no. 11, pp. 1045–1053, 2014. [Online]. Available: <https://doi.org/10.1177/0022034514552491>
- [3] N. Kassebaum *et al.*, “Global burden of untreated caries: A systematic review and metaregression,” *J. Dental Res.*, vol. 94, no. 5, pp. 650–658, 2015. [Online]. Available: <https://doi.org/10.1177/0022034515573272>
- [4] R. I. Garcia *et al.*, “Relationship between periodontal disease and systemic health,” *Periodontology*, vol. 25, no. 1, pp. 21–36, 2001. [Online]. Available: <https://onlinelibrary.wiley.com/doi/abs/10.1034/j.1600-0757.2001.22250103.x>
- [5] 2018. [Online]. Available: [https://www.dh.gov.hk/english/statistics/statistics\\_hs/files/Health\\_Statistics\\_pamphlet\\_E.pdf](https://www.dh.gov.hk/english/statistics/statistics_hs/files/Health_Statistics_pamphlet_E.pdf)
- [6] D. Ericson, E. Kidd, D. McComb, I. Mjör, and M. J. Noack, “Minimally invasive dentistry concepts and techniques in cariology,” *Oral Health Preventive Dentistry*, vol. 1, no. 1, pp. 59–72, 2003.
- [7] P. Kumar, P. Dixit, V. Kalaivani, and K. Rajapandian, “Future advances in robotic dentistry,” *J. Dental Health Oral Disorder Theory*, vol. 7, no. 3, 2017, Art. no. 00241.
- [8] M. Rawtiya, K. Verma, P. Sethi, and K. Loomba, “Application of robotics in dentistry quick response code,” *Indian J. Dental Adv.*, vol. 6, pp. 1700–1706, 2014.
- [9] T. Tanzawa *et al.*, “Medical emergency education using a robot patient in a dental setting,” *Eur. J. Dental Educ.*, vol. 17, no. 1, pp. e114–e119, 2013. [Online]. Available: <https://onlinelibrary.wiley.com/doi/abs/10.1111/j.1600-0579.2012.00770.x>
- [10] T. Tanzawa *et al.*, “Introduction of a robot patient into dental education,” *Eur. J. Dental Educ.*, vol. 16, no. 1, pp. e195–e199, 2012.
- [11] H. Takanobu, A. Takanishi, and I. Kato, “Design of a mastication robot mechanism using a human skull model,” in *Proc. IEEE/RSJ Int. Conf. Intell. Robot. Syst.*, Jul. 1993, vol. 1, pp. 203–208.
- [12] H. U. Takanobu and A. Takanishi, “Dental robotics and human model,” in *Proc. 1st Int. IEEE EMBS Conf. Neural Eng.*, Mar. 2003, pp. 671–674.
- [13] Z. Haidar, “Autonomous robotics: A fresh era of implant dentistry is a reality!” *J. Oral Res.*, vol. 6, no. 9, pp. 230–231, 2017. [Online]. Available: <http://www.jorales.com/index.php/JOR/article/view/jorales.2017.072>
- [14] W. Y. Lam *et al.*, “A 2-part facebow for CAD-CAM dentistry,” *J. Prosthetic Dentistry*, vol. 116, no. 6, pp. 843–847, 2016.
- [15] W. Y. Lam *et al.*, “A clinical technique for virtual articulator mounting with natural head position by using calibrated stereophotogrammetry,” *J. Prosthetic Dentistry*, vol. 119, no. 6, pp. 902–908, 2018.
- [16] W. Y. Lam, R. T. Hsung, L. Y. Cheng, and E. H. Pow, “Mapping intraoral photographs on virtual teeth model,” *J. Dentistry*, vol. 79, pp. 107–110, 2018.
- [17] G. Kim, H. Seo, S. Im, D. Kang, and S. Jeong, “A study on simulator of human-robot cooperative manipulator for dental implant surgery,” in *Proc. IEEE Int. Symp. Ind. Electron.*, 2009, pp. 2159–2164.
- [18] J. Jiang and Y. Zhang, “Application of robot to tooth-arrangement and dental implantology,” *Jiqiren(Robot)*, vol. 34, no. 5, pp. 634–640, 2012.
- [19] 2017. [Online]. Available: <https://ap.dental-tribune.com/news/first-ever-robot-led-dental-surgery-pe rformed-in-china/>
- [20] 2016. [Online]. Available: [https://www.universal-robots.com/media/50588/ur5\\_en.pdf](https://www.universal-robots.com/media/50588/ur5_en.pdf)
- [21] N. Delson and H. West, “Bracing to increase the natural frequency of a manipulator: Analysis and design,” *Int. J. Robot. Res.*, vol. 12, no. 6, pp. 560–571, 1993.
- [22] J. Y. Lew and W. J. Book, “Bracing micro/macro manipulators control,” in *Proc. IEEE Int. Conf. Robot. Automat.*, 1994, pp. 2362–2368.
- [23] W. J. Book, S. Le, and V. Sangveraphunsi, “Bracing strategy for robot operation,” in *Theory and Practice of Robots and Manipulators*. New York, NY, USA: Springer, 1985, pp. 179–185.
- [24] Z. Sun, Z. Wang, and S. J. Phee, “Elongation modeling and compensation for the flexible tendon-sheath system,” *IEEE/ASME Trans. Mechatronics*, vol. 19, no. 4, pp. 1243–1250, Aug. 2014.
- [25] T. N. Do *et al.*, “Dynamic friction-based force feedback for tendon-sheath mechanism in notes system,” *Int. J. Comput. Elect. Eng.*, vol. 6, pp. 252–258, 2014.
- [26] M. Khoshnam and R. V. Patel, “Tendon-sheath analysis for modeling and control of steerable ablation catheters,” in *Proc. IEEE Int. Conf. Adv. Intell. Mechatronics*, 2016, pp. 1585–1590.
- [27] T. Do, T. Tjahjowidodo, M. Lau, T. Yamamoto, and S. Phee, “Hysteresis modeling and position control of tendon-sheath mechanism in flexible endoscopic systems,” *Mechatronics*, vol. 24, no. 1, pp. 12–22, 2014.
- [28] J. Li, Y. Lam, T. Hsung, E. Pow, and Z. Wang, “A customizable, compact robotic manipulator for assisting multiple dental procedures,” in *Proc. IEEE Int. Conf. Adv. Robot.*, 2018, pp. 720–725.
- [29] J. Zhou, S. Chen, and Z. Wang, “A soft-robotic gripper with enhanced object adaptation and grasping reliability,” *IEEE Robot. Automat. Lett.*, vol. 2, no. 4, pp. 2287–2293, Oct. 2017.
- [30] J. Zhou, J. Yi, X. Chen, Z. Liu, and Z. Wang, “BCL-13: A 13-DOF soft robotic hand for dexterous grasping and in-hand manipulation,” *IEEE Robot. Automat. Lett.*, vol. 3, no. 4, pp. 3379–3386, Oct. 2018.
- [31] P. Polygerinos *et al.*, “Soft robotic glove for combined assistance and at-home rehabilitation,” *Robot. Auton. Syst.*, vol. 73, pp. 135–143, 2015.
- [32] P. Polygerinos *et al.*, “Modeling of soft fiber-reinforced bending actuators,” *IEEE Trans. Robot.*, vol. 31, no. 3, pp. 778–789, Jun. 2015.
- [33] Z. Wang, P. Polygerinos, J. T. B. Overvelde, K. C. Galloway, K. Bertoldi, and C. J. Walsh, “Interaction forces of soft fiber reinforced bending actuators,” *IEEE/ASME Trans. Mechatronics*, vol. 22, no. 2, pp. 717–727, Apr. 2017.